Available online at www.sciencedirect.com
SCIENCE DIRECT®
ELSEVIER
International Journal of Multiphase Flow 31 (2005) 957–967
International Journal of Multiphase Flow
www.elsevier.com/locate/ijmulflow

Brief communication

Confined fluidized bed—model and experiments

L. Moldavsky, A. Goldshtein, K. Shuster, M. Fichman, D. Pnueli, M. Shapiro *, C. Gutfinger

Faculty of Mechanical Engineering, Technion—Israel Institute of Technology, Haifa 32000, Israel

Received 25 June 2004; received in revised form 22 March 2005

1. Introduction

Fluidized bed technology is widely used in many engineering applications dealing with heat and mass transfer processes between solids and liquids. Fluidized beds are commonly used in industry for various purposes, e.g., catalytic reactions, gasification and combustion of solid fuels, drying of bulk materials, calcination and other treatments of ores, etc.

The rate of heat and mass transfer in fluidized beds depends on the fluidizing velocity; the higher the velocity through the bed, the more intensive the heat and mass transfer to the fluidized particles. In many traditional types of devices the fluidizing velocity u is restricted by the maximal value u_t that which would carry all the solid particles out of the device. Alternatively, when the outlet is blocked by a porous cap, in the regime where $u > u_t$ all the solid particles pack at this cap. For several industrial processes, such as catalytic cracking of oil, coal combustion and gasification, calcination of alumina and others (see Reh, 1986; Comtractor and Chaoki, 1990), where high rates of heat and mass transfer are required, standard fluidized bed devices are not sufficiently effective and circulating fluidized beds, also known as fast beds, are used extensively. In fast fluidized beds, the conveyed material is returned to the bottom of the bed. Such fast fluidized beds have certain disadvantages as compared to ordinary fluidized beds, namely, the additional cost for the solid particles return scheme, the smaller residence time, and the restriction on their productivity imposed by the transport velocity. A wide review of fluidized beds is given by Jackson (2000).

* Corresponding author. Tel.: +972 4 8293 185; fax: +972 4 8324 533.
E-mail address: mersm01@tx.tecnion.ac.il (M. Shapiro).

0301-9322/$ - see front matter
doi:10.1016/j.ijmultiphaseflow.2005.03.004

A Superfluidized Bed (SFB) process has been suggested by Fichman et al. (1995), which overcomes some of these shortcomings. In the SFB process a special vibrating grid is placed at the top of the bed, preventing the particles from leaving the device, no matter how high the carrier gas velocity. If the grid does not vibrate a porous plug of particles may form beneath it at high gas velocities, thus reducing the intensity of heat and mass transfer processes in the bed. The vibrations of the grid prevent the formation of the porous plug by sending the particles back into the fluidizing chamber, and thus retaining the beneficial properties of the fluidized bed. Along with the advantages of the SFB process there is an obvious disadvantage of the added complexity of the vibrating grid. Hence, a study of a non-vibrating fluidized bed is of practical interest.

Even when the grid does not vibrate, there are situations when no stable plug is formed in the bed confined by the grid. This usually happens when the gas velocity is sufficiently high to carry upward single particles, but not high enough to carry clusters of particles, or sustain a stable inverted packed bed.

The present study investigates particle accumulation at the confining grid in the absence of vibrations. During this process the fluidized bed coexists with a packed bed on top of it. Experimental data are presented and a model for the confined bed process is suggested.

2. Experimental results

The experimental system is shown schematically in Fig. 1. It consists of a closed loop, a transparent fluidized bed, and a centrifugal blower that circulates the air through it. The inner diameter of the bed is $D = 0.11$ m. The blower is driven by a DC motor power with variable speed drive, and can provide a maximal flow velocity inside the bed of 26 m/s. The velocity of the gas is measured in the connecting tube by a thermo-anemometer, from which the velocity in the bed is calculated.

The fluidized bed is formed inside a Plexiglas tube of 11 cm inner diameter. Two horizontal grids are placed inside the tube, and the space between them constitutes the confined bed chamber. The position of the bottom grid is fixed. The upper grid can be moved up and down, thereby changing the height, H, of the confined bed. Water manometers measure the pressure at two points in the connecting tubes, before and after the confined bed chamber. The granular material in the bed consists of small plastic spheres with the diameter $d = 4.1$ mm and the density $\rho_p = 1100\ \mathrm{kg/m^3}$.

The experiments were performed as follows. A mass M of spheres, comprising the granular bed, was loaded into the transparent chamber such that the initial height of the layer of the spheres at rest, i.e., the height of the initial packed bed, was h_0. The valve in the tube was gradually opened and the velocity of the air slowly increased. A maximal flow velocity was thus reached. The flow rate was then slowly decreased to zero. The part of the run in which the flow velocity is increased is termed as the loading period, and that in which the flow is decreased is the unloading period. The gas flow velocity and the pressure drop were measured during the loading and the unloading periods, and the state of the particles in the bed was recorded by a video camera. The various runs vary in their height of the confined bed, H, the height of the packed bed, h_0, and the maximal flow velocity attained.

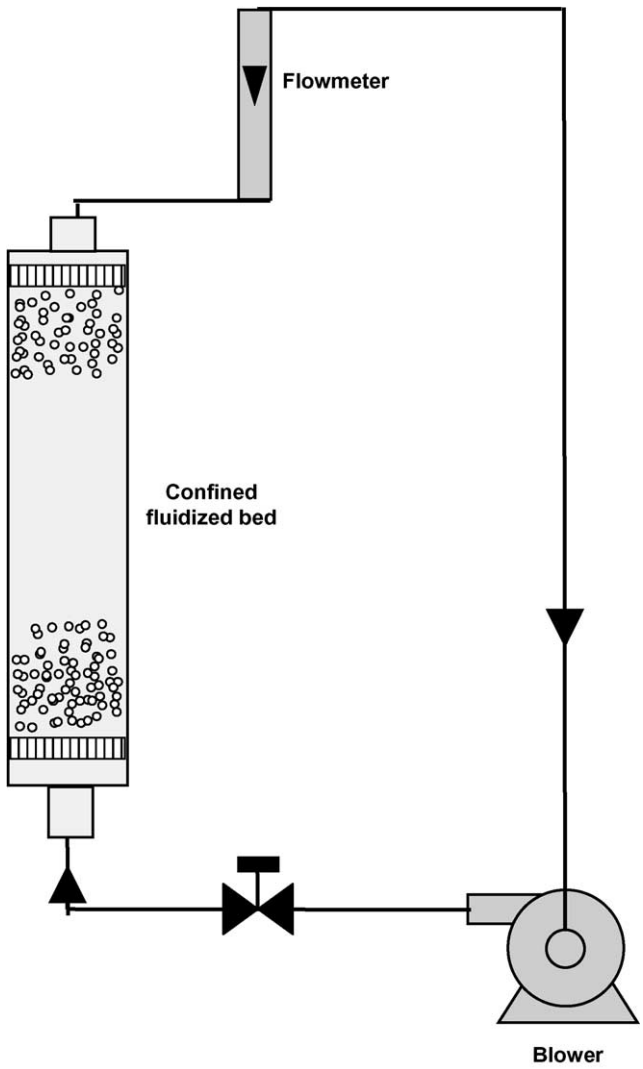

Fig. 1. Schematic of experimental set-up.

During the loading part of the experiments the bed passes through three stages, as illustrated in Fig. 2. At first the solid particles form a fluidized bed and do not interact with the upper grid, Fig. 2a. As the flow velocity increases, the bed expands, until the uppermost particles begin to touch the upper grid and stick to it, and the second stage begins. Now, part of the solid particles form a plug at the upper grid, whereas the other particles are fluidized in the space below the plug (Fig. 2b). The void fraction in the plug differs significantly from that in the fluidized part of the bed, and the boundary between the two regimes is easily observed (Fig. 2b). With further increase in the fluid velocity more particles reach the plug until all the particles in the bed gather at the upper grid (Fig. 2c), leading to the third stage, which is the inverted packed bed. This inverted packed bed state is now insensitive to moderate decrease or increase in the speed of the flow, and the void

Fig. 2. Photographs of different states of a confined fluidized bed (plastic spheres, $h_0 = 10d$, $d = 0.0041$ m): (a) fluidized bed state; (b) plug state; (c) inverted packed bed state.

fraction in the plug is constant. The pressure drop over the bed and the velocity of the air flow through the bed are measured for different bed heights, h_0, and different confined bed heights, H. The measured values are shown in Figs. 3 and 4. Fig. 3 is for $h_0 = 0.0205$ m and a velocity range chosen such that the inverted packed layer at the upper grid contains all the particles in the bed. Fig. 3 is for $h_0 = 0.041$ m and a velocity range determined by the maximum output of the blower.

As seen in Fig. 3, the velocity corresponding to the formation of the inverted packed layer is independent of the height of the bed, H, and for the plastic spheres of diameters of 4.1 mm used in the experiments this value is 11–12 m/s. Another feature shown is that during the velocity decrease (the upper branch of the curves) the pressure drop is higher than during the increase, shown in the lower branch. Hence, the pressure depends not only on the velocity but also on the history of the process. i.e., whether it is measured during the loading (the lower branch) or unloading (the upper branch). It is also noted that the upper branches for all the curves presented in Fig. 3 are practically the same, and depend just on the size of the plug formed.

Fig. 4 presents the pressure drop for a thicker bed, $h_0 = 0.041$ m. The maximal pressure drop here is restricted by the maximal output of the blower, which comes out to be $\Delta p_{\max} = 800$ Pa. The packed bed stage has not been reached for this deeper bed. However, all of the curves in the Fig. 4 also have two branches and show dependence on the history of the loading, as in Fig. 3.

During the loading stage the plug of the particles at the upper grid grows with time and with the increase in velocity. During the unloading stage the inverted packed part of the bed remains packed and does not change. Since most of the pressure drop takes place in the packed part of

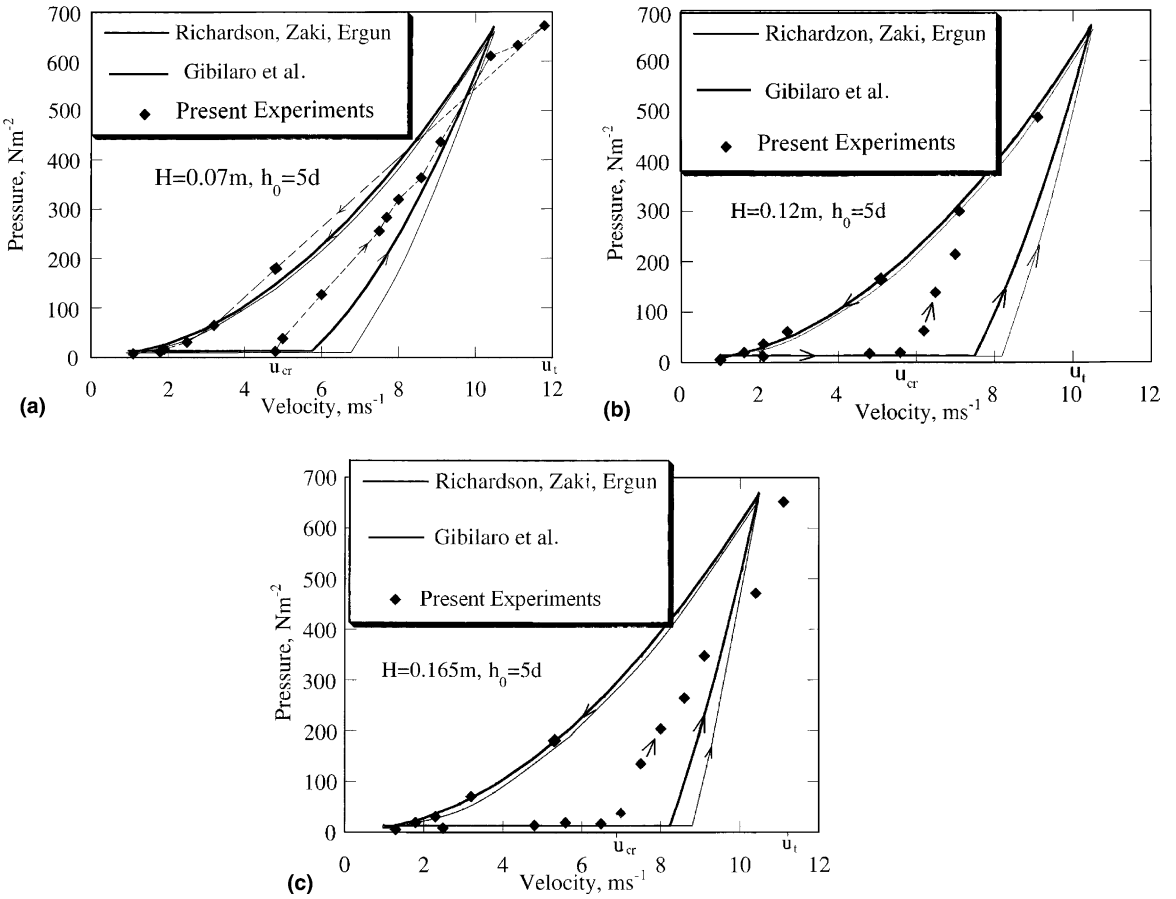

Fig. 3. Pressure drop across a bed of plastic spheres ($d = 0.0041$ m, $h_0 = 5d = 0.021$ m) versus gas velocity; experimental and theoretical results. Solid squares—experimental data, thin curves—predictions of the model based on the Gibilaro et al. (1985) approximation, thick curves—predictions of the model based on the Richardson and Zaki (1954) and Ergun (1952) approximations. (a) $H = 0.07$ m, (b) $H = 0.12$ m, (c) $H = 0.165$ m.

the bed, the difference between the two branches in the figures can be qualitatively explained by the differences in heights of the packed parts of the bed. Some more comments are presented in Section 4.

3. Theoretical model

To simplify the analysis a constant mean void fraction, ε, is assumed for each regime of flow. As seen in Fig. 5, the particles may either stay at the bottom of the bed, float in the fluidized part of the bed, or be inverted packed below the upper grid. Each of these regions is assumed to have its own constant average void fraction. Due to this assumption, we may use known empirical relations for the pressure drop in each region. Below we present several existing empirical models

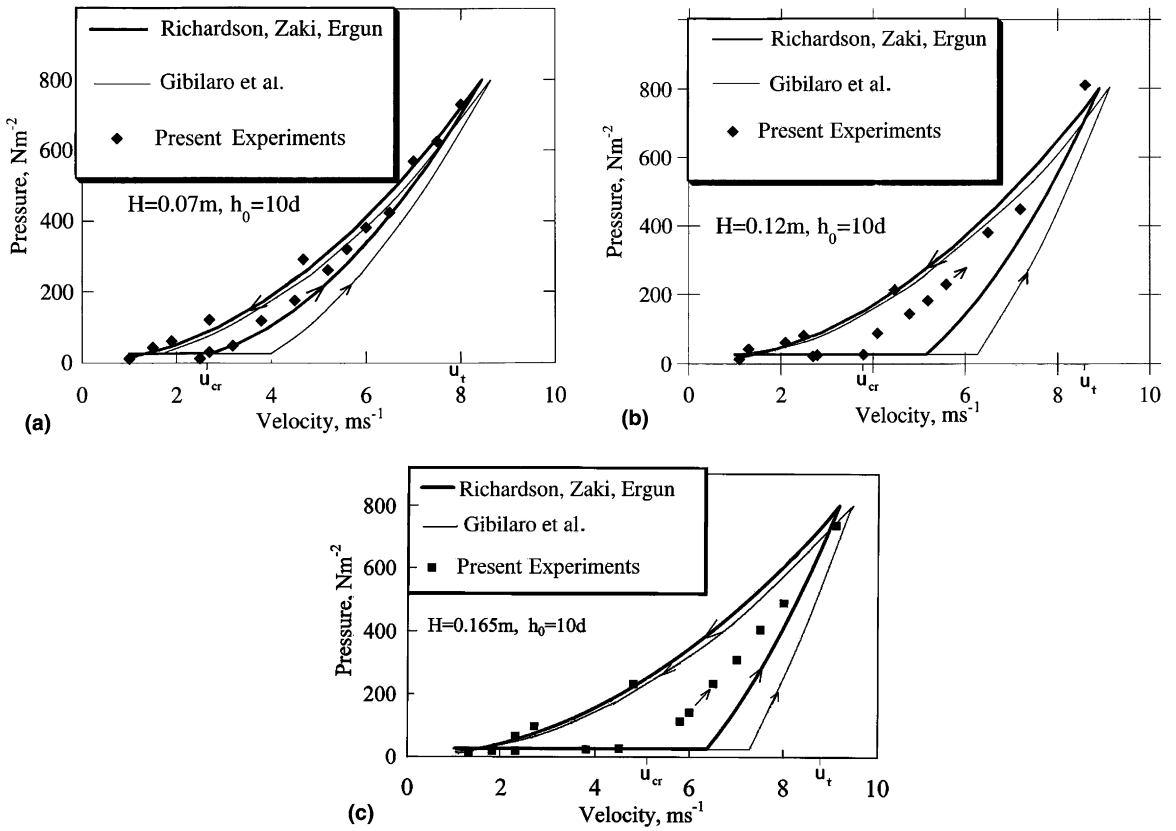

Fig. 4. Pressure drop across a bed of plastic spheres ($d = 0.0041$ m, $h_0 = 10d = 0.041$ m) versus gas velocity; experimental and theoretical results. Solid squares—experimental data, thin curves—predictions of the model based on the Gibilaro et al. (1985) approximation, thick curves—predictions of the model based on the Richardson and Zaki (1954) and Ergun (1952) approximations. (a) $H = 0.07$ m, (b) $H = 0.12$ m, (c) $H = 0.165$ m.

and relationships and show how they can be combined to form a theoretical model for the confined fluidized bed.

Since the mass of a bed does not change in each experiment the mass conservation condition may be written in terms of the confined bed's height h_f and ε

for a fluidized bed:

$$h_f(1-\varepsilon) = h_0(1-\varepsilon_0) = 4M/\rho_p \pi D^2 \tag{1}$$

for a confined bed:

$$h_f(1-\varepsilon) + h_p(1-\varepsilon_0) = h_0(1-\varepsilon_0), \tag{2}$$

where the subscripts f and p denote fluidized bed and the plug region, respectively and subscript 0 refers to the properties of the whole bed in the packed regime.

A fluidized bed can exist if the height, h_f is less than the distance between the grids. When the particles of the fluidized bed approach the upper grid they begin to "stick" to it forming a plug.

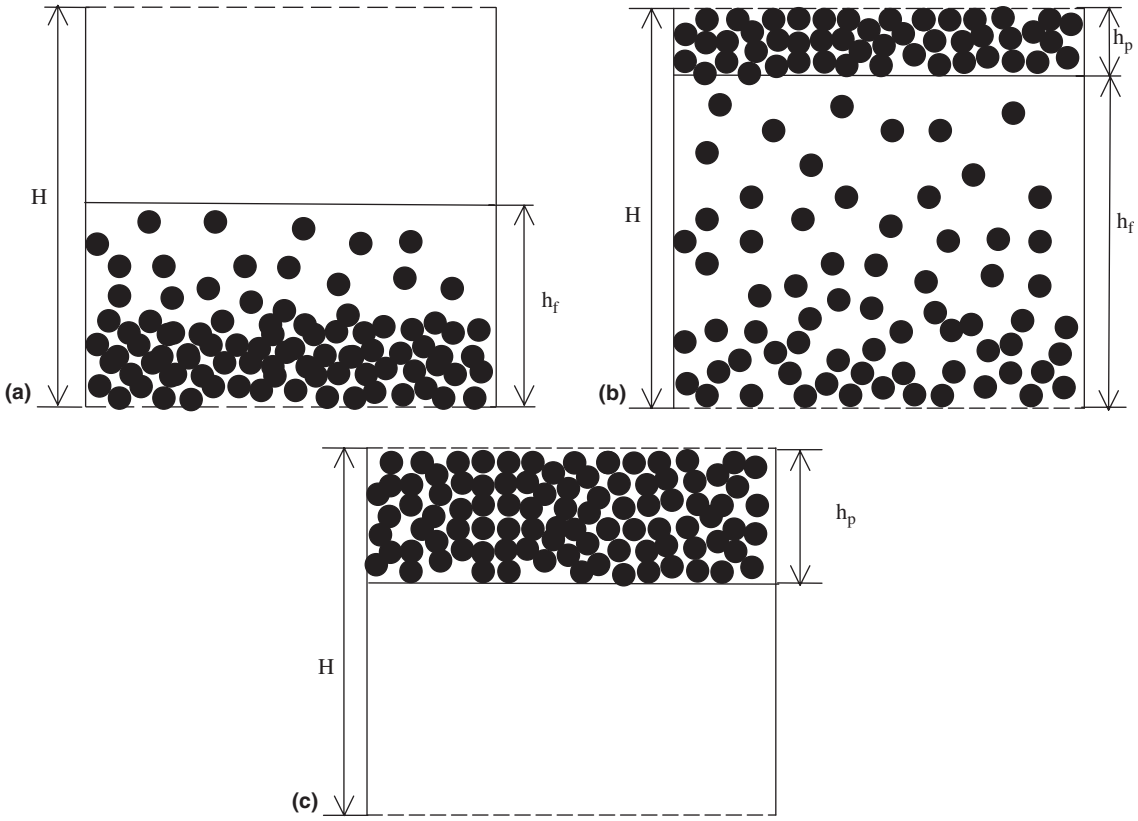

Fig. 5. Schematic of the different states of a confined fluidized bed: (a) fluidized bed; (b) packed bed; (c) inverted packed bed.

The height H of the bed is the sum of the heights of the fluidized and plug regions (inverted bed) (see Fig. 5b)

$$h_f + h_p = H \tag{3}$$

There are several empirical expressions for the calculation of the pressure drop across the bed. For a bed of packed spheres with $\varepsilon \leqslant 0.4$ the Ergun equation

$$\Delta P_E = h_p \left[150 \frac{(1-\varepsilon)^2}{\varepsilon^3} \frac{\mu u}{d^2} + 1.75 \frac{1-\varepsilon}{\varepsilon^3} \frac{\mu u^2}{d} \right], \tag{4}$$

with μ being the air viscosity, gives reliable results. Richardson and Zaki (1954) have shown that the following simple expression:

$$\frac{u}{u_t} = \varepsilon^n \tag{5}$$

could be used to relate the sedimentation or fluidization velocity, u, the void fraction ε, and the terminal particle velocity, u_t in the fluid. The terminal velocity may be found equating the drag force on a single particle to its effective weight

$$C_D \frac{\rho u_t^2}{2} \frac{\pi d^2}{4} = \frac{\pi d^3}{6} (\rho_p - \rho) g, \tag{6}$$

where g is the acceleration due to gravity and for large Reynolds numbers $C_D \approx 0.44$.

The exponent n in Eq. (5) was given by Khan and Richardson (1989) in terms of the ratio of the particle-to-vessel diameter (d/D) and the Galileo number, $Ga = d^3 \rho g (\rho_p - \rho)/\mu^2$

$$\frac{4.8 - n}{n - 2.4} = 0.0043 Ga^{0.57} \left[1 - 1.24 \left(\frac{d}{D} \right)^{0.27} \right]. \tag{7}$$

Expressions (5)–(7) enable to calculate the void fraction in the fluidized bed for a given velocity. The pressure drop across the bed is found by equating it to the weight per unit area of the particles in the fluidized bed

$$\Delta P_f = \rho_p (1 - \varepsilon) g h_f. \tag{8}$$

There were many attempts to derive a single correlation which is valid for the wide range of void fractions from dilute fluidized suspensions and up to the packed bed state. For a discussion of this topic see the paper by Khan and Richardson (1990). One of such correlations was suggested by Gibilaro et al. (1985)

$$\Delta P = \left(\frac{17.3}{Re} + 0.336 \right) \frac{\rho u^2 H}{d} (1 - \varepsilon) \varepsilon^{-4.8} \tag{9}$$

This correlation had been claimed to be applicable in a wide range of the void fractions, ε from 0.4 to 1, covering fluidized suspensions as well as fixed beds of height H. This simple correlation does not contain any fitting parameters and is independent of the bed diameter.

Below we show how to use the above correlations to calculate the velocity–pressure relationship for all three regimes. For the first stage (fluidized bed) the pressure drop across the bed is equal to the bed weight per unit area. Combining (1) and (8) one obtains

$$\Delta P_f = \rho_p (1 - \varepsilon_0) g h_0. \tag{10}$$

This pressure drop is independent of the gas velocity until the latter changes between the minimal fluidizing velocity, u_{mf} and the terminal velocity, u_t. This is true if the vessel containing the bed is unconfined from above. In our case, Eq. (10) holds for gas velocities smaller than the critical velocity, u_{cr}, i.e., the one at the onset of plug formation on the upper grid. The latter value characterizes the transition from the first stage (fluidized bed) to the second one, where the fluidized region coexists with the plug region. This transition happens when the fluidized bed fills the whole volume between the grids i.e.,

$$h_f = H. \tag{11}$$

This condition may also be derived from Eq. (3) for the confined fluidized bed by setting $h_p = 0$. We define a critical void fraction as the one corresponding to the onset of plug formation. Using mass conservation, Eq. (1), together with Eq. (11) the critical void fraction is given as

$$\varepsilon_{cr} = 1 - (1 - \varepsilon_0) h_0 / H. \tag{12}$$

Substitution of this value into Eq. (5) yields the critical velocity predicted by the model of Richardson and Zaki (1954) in the form

$$u_{cr} = \varepsilon_{cr}^{n} u_t. \tag{13}$$

Another prediction of the critical velocity may be obtained from the model of Gibilaro et al. (1985). Eqs. (9) and (11) yield after some algebra the following expression:

$$g\rho_p = \left(17.3 + 0.336\frac{\rho u_{cr} d}{\mu}\right)\frac{\mu u_{cr}}{d}\varepsilon_{cr}^{-4.8} \tag{14}$$

The solution of this equation yields u_{cr}.

We assume that for $u > u_{cr}$ (or $\varepsilon > \varepsilon_{cr}$) the plug stage begins. In this stage, the pressure drop across the bed is equal to the sum of the pressure drops across the fluidized and inverted packed parts of the bed

$$\Delta P = \Delta P_f + \Delta P_p. \tag{15}$$

To use this expression one needs to calculate the heights, h_f, h_p, and the void fraction, ε within the fluidized part of the bed (see Fig. 3b). For the Richardson and Zaki model, it may be done by solving a system of three equations (2), (3), (5) for a fixed velocity, u and a given n (calculated from Eq. (7)). After that the first term in Eq. (15) is calculated from Eq. (7) whereas the second one from Ergun's correlation, Eq. (4). The second stage, where the fluidized and plug regimes coexist, terminates when $u = u_t$, and all the particles are amassed in the plug.

In order to calculate the pressure drop in Eq. (15) on the basis of the correlation of Gibilaro et al. (9), it is convenient to equate Eqs. (8) and (9) leading to

$$\rho_p g = \left(\frac{17.3}{Re} + 0.336\right)\frac{\rho u^2}{d}\varepsilon^{-4.8}. \tag{16}$$

This equation may now be solved to give ε. For the calculated ε, the heights of the fluidized and packed parts of the bed may be easily calculated from Eqs. (2) and (3). After that, both terms in the right-hand-side of Eq. (15) may be calculated on the basis of Eq. (9), using different values of ε corresponding to the respective regimes. It is worth mentioning that the correlation of Gibilaro et al. (9) yields the same terminal velocity for large Reynolds numbers as Eq. (6).

In the third stage (inverted packed bed) we used the two models for the description of the velocity–pressure dependence, namely those of Ergun (Eq. (4)) and Gibilaro et al. (Eq. (9)). In the following section we compare the above mathematical models with our experimental results.

4. Comparison between experiments and theoretical results

To verify the applicability of the above mathematical models we adapt them to our experimental conditions. Both models predict that the third stage of the inverted packed bed begins when the superficial velocity u reaches the terminal velocity u_t. This statement is in good agreement with the experimental data presented in Fig. 4. One can see that all three curves describing the loading process terminate practically at the same point of the pressure-velocity diagram. The maximal pressure achieved in these experiments, when all particles were collected on the upper grid, is about

650 N/m^2 (see Fig. 4). This pressure is associated with the packed bed state when $\varepsilon = \varepsilon_0$ Since Eqs. (4) and (9) for a packed bed are very sensitive to the value of the void fraction ε, we used ε_0 as an adjustable parameter. Specifically, ε_0 was chosen as the one corresponding to

$$\Delta P = 650 \text{ N/m}^2 \tag{17}$$

where ΔP_t is the pressure drop calculated for the terminal gas velocity, $u = u_t$, and the void fraction as that of the packed state $\varepsilon = \varepsilon_0$. Using directly measured parameters characterizing our experimental conditions, namely $g = 9.8$ m/s^2, $d = 0.0041$ m, $\rho_p = 1100$ kg/m^3, $\rho = 1.2$ kg/m^3, $\mu = 0.18 \times 10^{-4}$ N s/m^2, $D = 0.11$ m, one obtains from Eq. (6) the terminal velocity as $u_t \approx 10.5$ m/s. Substituting this value together with the height of the packed layer, $5d$ into Eqs. (4) and (9), respectively, one obtains two different relationships for ΔP_t. Substitution of these relationships into the right-hand-side of equation (17) yields two different algebraic equations for the still unknown void fraction ε_0, which yield $\varepsilon_0 = 0.4$ for the Richardson and Zaki model, and $\varepsilon_0 = 0.437326$ for the model of Gibilaro et al. When ε_0 is specified the model of Gibilaro et al., is completely defined, while for the other model one needs the index n, which for our experimental conditions Eq. (7) yields as $n = 3.07819$.

The curves in Figs. 3 and 4 present pressure-velocity dependencies calculated for both models and our experimental data. The lines represent the expressions of Richardson and Zaki, Ergun and Gibilaro et al., respectively, while the points are our experimental data. In each figure one can distinguish three curves forming a closed triangle. The horizontal constant pressure line depicts the fluidized state, while the curve with the monotonic increase in pressure describes the stage of plug formation up to the inverted packed bed state. The last curve with the decreasing pressure is for the unloading stage. The theories and the experiments indicate the hysteresis-type behavior of the pressure-velocity plot.

One can see that qualitatively both models describe correctly the pressure-velocity relation during the various stages that the confined bed is undergoing. Each model predicts the transition from the initial fluidized stage, through the plug formation stage and to the final inverted packed bed stage in a monotonic manner in agreement with the experimental data. In general, the combination of the Richardson–Zaki and Ergun equations fits the experimental data better that the expression of Gibilaro et al. Both theories fit the data quite well during the fluidization and the unloading stages, while during the plug formation stage both theories underestimate the pressures measured experimentally.

The measured terminal velocity shown in Fig. 3 is 9–12 m/s, while for the deeper inverted bed of Fig. 4 it is 8–9.5 m/s. The velocity calculated from Eq. (6) is $u_t = 10.56$ m/s, which is rather close to the velocities measured experimentally. The slightly lower velocities for the deeper inverted bed of Fig. 4 may indicate that in the shorter travel distance the particles may not have reached the terminal velocity.

5. Conclusions

At small velocities (first stage) the confined bed operates in a regular fluidized bed regime and the pressure drop across it is constant. At higher velocities (second stage) particles accumulate at the upper grid and form a plug there. Further velocity increase creates inverted packed bed (third

stage). In the course of unloading (reducing velocity) the pressure drop exceeds that prevailing during velocity increase, exhibiting thus a hysteresis-type behavior.

Two variants of theoretical model of the confined bed were developed: one based on the correlation of Richardson–Zaki and Ergun equation and the other—based on the Gibilaro et al.'s correlation. Each model predicts the transition from the initial fluidized stage, through the plug formation stage and to the final inverted packed bed stage in a monotonic manner in agreement with the experimental data. Furthermore the models predict that the third stage of the inverted packed bed begins when the superficial velocity u reaches the terminal velocity u_t. This is in good agreement with the experimental data presented in Fig. 4. In general, the combination of the Richardson–Zaki and Ergun equations fits the experimental data better that the model based on expression of Gibilaro et al. Both theories fit the data quite well during the fluidization and the unloading stages, while during the plug formation stage both theories underestimate the pressures measured experimentally.

References

Comtractor, R.M., Chaoki, J., 1990. Circulating fluidized bed as a catalytic reactor. In: Basu, P., Horio, M., Chaoki, J. (Eds.), Circulating Fluidized Bed Technology, vol. III. Pergamon Press, Oxford, p. 39.

Ergun, S., 1952. Fluid flow through packed columns. Chem. Eng. Prog. 48, 89.

Fichman, M., Goldshtein, A., Gutfinger, C., Moldavsky, L., Pnueli, D., Shapiro, M., 1995. Method and Apparatus for Combined Fluid Vibrofluidized Bed (A Superfluidized Bed Method and Apparatus). Israel, Patent No. 112687.

Gibilaro, G.L., Felice, R.Di., Waldram, S.P., Foscolo, P.U., 1985. Generalized friction factor and drag coefficient correlations for fluid-particle interaction. Chem. Eng. Sci. 40, 1817.

Jackson, R., 2000. The Dynamics of Fluidized Beds. Cambridge University Press, NY.

Khan, A.R., Richardson, J.F., 1990. Pressure gradient and friction factor for sedimentation and fluidization of uniform spheres and liquids. Chem. Eng. Sci. 45, 255.

Khan, A.R., Richardson, J.F., 1989. Fluid-particle interactions and flow characteristics of fluidized beds and settling suspensions of spherical particles. Chem. Eng. Commun. 78, 111.

Reh, L., 1986. The circulating fluidized bed reactor: a key to efficient gas/solid processing. In: Basu, P. (Ed.), Circulating Fluidized Bed Technology, vol. I. Pergamon Press, Oxford, p. 105.

Richardson, J.F., Zaki, W.N., 1954. Sedimentation and fluidization. Trans. Inst. Chem. Eng. 32, 38.